Robotica (2014) volume 32, pp. 165–174. © Cambridge University Press 2013
doi:10.1017/S0263574713000660

Laser interferometry measurements based calibration and error propagation identification for pose estimation in mobile robots

Paulo A. Jiménez* and Bijan Shirinzadeh

Robotics and Mechatronics Research Laboratory (RMRL), Department of Mechanical and Aerospace Engineering, Monash University, Clayton, Victoria, Australia

(Accepted June 17, 2013. First published online: August 6, 2013)

SUMMARY

A widely used method for pose estimation in mobile robots is odometry. Odometry allows the robot in real time to reconstruct its position and orientation from the wheels' encoder measurements. Given to its unbounded nature, odometry calculation accumulates errors with quadratic increase of error variance with traversed distance. This paper develops a novel method for odometry calibration and error propagation identification for mobile robots. The proposed method uses a laser-based interferometer to measure distance precisely. Two variants of the proposed calibration method are examined: the two-parameter model and the three-parameter model. Experimental results obtained using a Khepera 3 mobile robot showed that both methods significantly increase accuracy of the pose estimation, validating the effectiveness of the proposed calibration method.

KEYWORDS: Mobile robots; Navigation; Robot localisation; Pose estimation and registration; Mechatronic systems.

1. Introduction

While navigating, a robot uses a kinematic model to estimate its current position. Encoders count the number of revolutions that the wheels make while moving. These readings and the geometry of the robot are used to calculate the displacement to provide the position of the robot. The accuracy of position depends on the accuracy of measurements taken and the accuracy of the parameters used in the model. Nevertheless, no mechanical system is ever manufactured perfectly. In general, uncertainties in robot's geometry and noise in sensors' measurements induce errors in the estimated localisation.

Errors can be broadly classified into systematic and non-systematic errors. Systematic errors are caused by inaccuracies in the manufacturing and assembly of the components (such as wheel diameters, motors and wheel misalignment). Non-systematic errors are caused by the random characteristics of the sensors and transducers and environmental effects. Non-systematic errors comprise of wheel slippage, couplings backlash, sensitivity of the material to temperature and noise. The combined error is constantly increasing, and assuming that the odometry readings are perfect would result in incorrect position estimates.

Approaches to odometry calibration can be broadly divided into off-line or on-line. Off-line calibration is mostly done by defining an expanded mobile robot kinematics model with calibration parameters and computing their values by performing appropriate experiments.[2–4] On-line odometry calibration is used to increase the pose estimation accuracy during mobile robot navigation or to estimate the random errors variance.[6,7] In the case of on-line odometry calibration, the calibration parameters convergence is crucial, just like the pose estimation accuracy. Both the convergence of the

* Corresponding author. E-mail: Paulo.Jimenez@monash.edu

https://doi.org/10.1017/S0263574713000660 Published online by Cambridge University Press

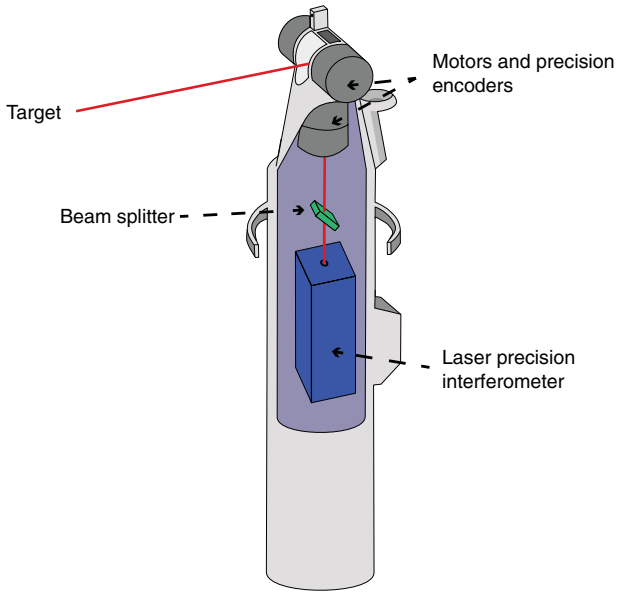


Fig. 1. (Colour online) Laser interferometry sensing layout.

parameters and accuracy of the pose estimation can be significantly improved if good initial values of the parameters are chosen.

In general, a good calibration method does not need a large testing space and it is not time-consuming. This study proposes a novel calibration method for a mobile robot based on laser interferometry measures. The proposed methodology aims to generate accurate results for a trajectory relative to an initial location. The robot also needs to be aware of its own odometric errors because these errors increase continuously. The consideration of odometric errors gives a more realistic view of the environment and, therefore, it has the potential of improved decision making in real-world situations. Therefore, this paper also proposes a method to identify the parameters of the error propagation.

The paper starts by briefly describing the laser interferometry principle. In Section 3, the error model is described and two models are proposed. Section 4 identifies the error propagation parameters that represent error awareness in a real-world scenario. Section 5 establishes the proposed laser interferometry methodologies. Section 6 introduces the experiments and presents the results obtained. Finally, in Section 7, conclusions are drawn and further research proposed.

2. Laser Interferometry Sensing Principle

Laser-interferometry-based sensing has been used to produce highly accurate results for many robotics systems.[1,9] The system tracks the target by sensing the offset of the incident and reflected beam, correcting the offset by adjusting the angles of the beam steering mechanism. A functional layout of the system is provided in Fig. 1.

In this layout, the laser beam travels to the interferometer, where it is split into a reference beam and a measurement beam. The measurement beam is then directed towards the target retro-reflector. The beam then hits the target retro-reflector and is reflected through 180° so that the reflected beam travels back parallel to the incident beam. If the beam does not hit the centre of the retro-reflector, it will be offset by an amount of error that constitutes the tracking error of the beam. The reference beam is compared with the returning measurement beam (whose frequency will be Doppler-shifted) to determine the distance between the target and the laser head. The angles of the tracking mirror axes are then provided by two high-precision encoders attached to each motor in the tracking mechanism. These values in conjunction with the measurement from the interferometer provide a measurement in spherical coordinates of the position of the robot relative to the system.

https://doi.org/10.1017/S0263574713000660 Published online by Cambridge University Press

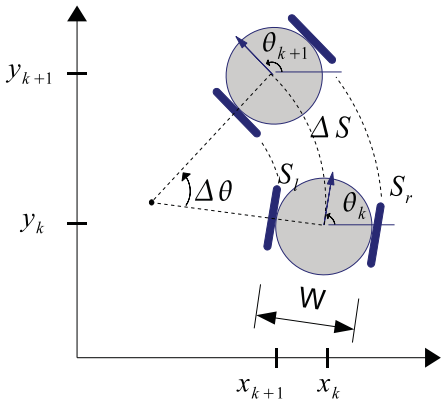


Fig. 2. (Colour online) Differential drive schematic representation.

3. Error Model Description

Odometry relies on tracking the current position using a series of measurements for each time interval Δt. Let us consider a differential drive mobile robot as shown in Fig. 2. The discrete form of the odometric navigation equation is given by

$$\begin{bmatrix} x_{k+1} \\ y_{k+1} \\ \theta_{k+1} \end{bmatrix} = \begin{bmatrix} x_k \\ y_k \\ \theta_k \end{bmatrix} + \begin{bmatrix} \frac{S_r+S_l}{2}\cos\left(\theta_k + \frac{S_r-S_l}{2W}\right) \\ \frac{S_r+S_l}{2}\sin\left(\theta_k + \frac{S_r-S_l}{2W}\right) \\ \frac{S_r-S_l}{W} \end{bmatrix}, \tag{1}$$

where S_r and S_l are the distances covered by the right and left wheels and W is the distance between its driven wheels. Suppose that during the time interval Δt the left and right wheel encoders show an increment (N_r, N_l), respectively. The incremental travel distance for the left and right wheels is derived according to

$$S_r = \frac{\pi D N_r}{n C_e}, \tag{2}$$

$$S_l = \frac{\pi D N_l}{n C_e}, \tag{3}$$

where D is the nominal wheel diameter, n is the gear ratio of the reduction and C_e is the encoder resolution. Alternatively, Eqs. (2) and (3) can be expressed in terms of the left and right speed by

$$S_r = V_r \Delta t, \tag{4}$$

$$S_l = V_l \Delta t. \tag{5}$$

True wheel encoder outputs are corrupted with errors and some kinematic parameters are not exactly known. Non-systematic errors are mostly of a stochastic nature and cannot be compensated. Systematic errors could be seen as a scaling factor, since they do not change during typical runs. Therefore, a proper calibration of the robot could reduce these errors significatively. A way to represent the error is to consider travelled distance and change in orientation in one time step by rewriting (1) into

$$\begin{bmatrix} x_{k+1} \\ y_{k+1} \\ \theta_{k+1} \end{bmatrix} = \begin{bmatrix} x_k \\ y_k \\ \theta_k \end{bmatrix} + \begin{bmatrix} c_d \frac{S_r+S_l}{2}\cos\left(\theta_k + c_r \frac{S_r-S_l}{2W}\right) \\ c_d \frac{S_r+S_l}{2}\sin\left(\theta_k + c_r \frac{S_r-S_l}{2W}\right) \\ c_r \frac{S_r-S_l}{W} \end{bmatrix}, \tag{6}$$

where c_d and c_r are the elements that compensate the distance and the orientation. Another approach is to consider the individual factors that create this error. Then, Eq. (1) can be rewritten to represent

https://doi.org/10.1017/S0263574713000660 Published online by Cambridge University Press

the mentioned error influence as

$$\begin{bmatrix} x_{k+1} \\ y_{k+1} \\ \theta_{k+1} \end{bmatrix} = \begin{bmatrix} x_k \\ y_k \\ \theta_k \end{bmatrix} + \begin{bmatrix} \frac{c_r S_r + c_l S_l}{2} \cos(\theta_k + \frac{c_r S_r - c_l S_l}{c_W 2W}) \\ \frac{c_r S_r + c_l S_l}{2} \sin(\theta_k + \frac{c_r S_r - c_l S_l}{c_W 2W}) \\ \frac{c_r S_r - c_l S_l}{c_W W} \end{bmatrix}, \tag{7}$$

where c_r and c_l are the parameters that compensate the radius of the each wheel and c_W is the parameter that compensates for the distance between wheels.

It has to be noticed that both sets of parameters represent systematic error in the distance and the orientation. Equations (6) and (7) are refereed here as the two-parameter and three-parameter models, respectively.

4. Error Propagation Identification

The entire path is defined as a set of segments, where the covariance is iteratively evaluated in order to obtain the covariance of the final state. The robot's pose uncertainty at stage k is described by a covariance matrix:

$$\mathbf{C_{P_k}} = \begin{bmatrix} \sigma_x^2 & \sigma_{yx} & \sigma_{\theta x} \\ \sigma_{xy} & \sigma_y^2 & \sigma_{\theta y} \\ \sigma_{x\theta} & \sigma_{y\theta} & \sigma_\theta^2 \end{bmatrix}. \tag{8}$$

The covariance propagation is based upon the linearisation of non-linear equations describing dependencies between the variables in the measurement process by Taylor series expansions and the computation of the proper Jacobian. The covariance matrix of the next stage $(k+1)$ is propagated as follows:

$$\begin{aligned} \mathbf{C_{P_{k+1}}} &= E\left\{(P_{k+1} - \bar{P}_{k+1})(P_{k+1} - \bar{P}_{k+1})^T\right\} \\ &\approx [\mathbf{\Phi} \quad \mathbf{\Gamma}] \begin{bmatrix} \mathbf{C_{P_k}} & 0 \\ 0 & \mathbf{C_{u_k}} \end{bmatrix} \begin{bmatrix} \mathbf{\Phi}^T \\ \mathbf{\Gamma}^T \end{bmatrix} \\ &= \mathbf{\Phi} \boldsymbol{C_{Pk}} \mathbf{\Phi}^T + \mathbf{\Gamma} \boldsymbol{C_{u_k}} \mathbf{\Gamma}^T, \end{aligned} \tag{9}$$

where $\mathbf{\Phi}$ is the system Jacobian given by

$$\mathbf{\Phi} = \begin{bmatrix} 1 & 0 & -\frac{\pi D(N_l+N_r)}{2C_e n} \sin\left(\theta - \frac{\pi D(N_l-N_r)}{(2C_e W n)}\right) \\ 0 & 1 & \frac{\pi D(N_l+N_r)}{2C_e n} \cos\left(\theta - \frac{\pi D(N_l-N_r)}{2C_e W n}\right) \\ 0 & 0 & 1 \end{bmatrix} \tag{10}$$

and $\mathbf{\Gamma}$ is the Jacobian of the input vector $[N_l \quad N_r]$:

$$\mathbf{\Gamma} = \begin{bmatrix} \frac{\pi D}{2C_e n} \cos\left(\theta - \frac{\pi D(N_l-N_r)}{2C_e W n}\right) - \frac{D^2\pi^2(N_l+N_r)}{4C_e^2 W n^2} \sin\left(\theta - \frac{\pi D(N_l-N_r)}{2C_e W n}\right), \\ \frac{\pi D}{2C_e n} \sin\left(\theta - \frac{\pi D(N_l-N_r)}{2C_e W n}\right) + \frac{D^2\pi^2(N_l+N_r)}{4C_e^2 W n^2} \cos\left(\theta - \frac{\pi D(N_l-N_r)}{2C_e W n}\right), \\ \frac{\pi D}{C_e W n}, \\ \frac{\pi D}{2C_e n} \cos\left(\theta - \frac{\pi D(N_l-N_r)}{2C_e W n}\right) + \frac{D^2\pi^2(N_l+N_r)}{4C_e^2 W n^2} \sin\left(\theta - \frac{\pi D(N_l-N_r)}{2C_e W n}\right) \\ \frac{\pi D}{2C_e n} \sin\left(\theta - \frac{\pi D(N_l-N_r)}{2C_e W n}\right) - \frac{D^2\pi^2(N_l+N_r)}{4C_e^2 W n^2} \cos\left(\theta - \frac{\pi D(N_l-N_r)}{2C_e W n}\right) \\ -\frac{\pi D}{C_e W n} \end{bmatrix}. \tag{11}$$

https://doi.org/10.1017/S0263574713000660 Published online by Cambridge University Press

Alternatively, Eqs. (10) and (11) can be represented in terms of the $[V_l \quad V_r]$ input vector by

$$\mathbf{\Phi} = \begin{bmatrix} 1 & 0 & -\frac{\Delta t(V_l+V_r)}{2}\sin\left(\theta - \frac{\Delta t(V_l-V_r)}{2W}\right) \\ 0 & 1 & \frac{\Delta t(V_l+V_r)}{2}\cos\left(\theta - \frac{\Delta t(V_l-V_r)}{2W}\right) \\ 0 & 0 & 1 \end{bmatrix} \tag{12}$$

and

$$\mathbf{\Gamma} = \begin{bmatrix} \frac{\Delta t}{2}\cos\left(\theta - \frac{\Delta t(V_l-V_r)}{2W}\right) - \frac{\Delta t^2(V_l+V_r)}{4W}\sin\left(\theta - \frac{\Delta t(V_l-V_r)}{2W}\right), \\ \frac{\Delta t}{2}\sin\left(\theta - \frac{\Delta t(V_l-V_r)}{2W}\right) + \frac{\Delta t^2(V_l+V_r)}{4W}\cos\left(\theta - \frac{\Delta t(V_l-V_r)}{2W}\right), \\ \frac{\Delta t}{W}, \\ \frac{\Delta t}{2}\cos\left(\theta - \frac{\Delta t(V_l-V_r)}{2W}\right) + \frac{\Delta t^2(V_l+V_r)}{4W}\sin\left(\theta - \frac{\Delta t(V_l-V_r)}{2W}\right) \\ \frac{\Delta t}{2}\sin\left(\theta - \frac{\Delta t(V_l-V_r)}{2W}\right) - \frac{\Delta t^2(V_l+V_r)}{4W}\cos\left(\theta - \frac{\Delta t(V_l-V_r)}{2W}\right) \\ -\frac{\Delta t}{W} \end{bmatrix}. \tag{13}$$

Since two separate motors and encoders are used to gather odometry information, it is possible to assume that the left and right inputs are uncorrelated. Then, $\mathbf{C_{u_k}}$ is defined as

$$\boldsymbol{C}_{\boldsymbol{u}_k} = \begin{bmatrix} \sigma_r(\cdot) & 0 \\ 0 & \sigma_l(\cdot) \end{bmatrix}, \tag{14}$$

where $\sigma_r(\cdot)$ and $\sigma_l(\cdot)$ are assumed to be functions of the input vector defined by

$$\sigma_r(\cdot) = \begin{cases} K_{rc} \\ K_{rl}\, N_r \quad or \quad K_{rl}\, V_r, \end{cases} \tag{15}$$

$$\sigma_l(\cdot) = \begin{cases} K_{lc} \\ K_{ll}\, N_l \quad or \quad K_{ll}\, V_l. \end{cases} \tag{16}$$

It has to be noticed that these functions (constant or lineal) are used to calculate the error propagation. Then, it is necessary to identify the parameters $[K_{rc} \quad K_{lc}]$ and $[K_{rl} \quad K_{ll}]$ in order to fine-tune the error propagation method. The error ellipse is calculated from the covariance matrix by projecting the ellipsoid onto a plane. This ellipse shows the area that contains the robot position within a level of probability. A standard error ellipse is centred on the nominal (x, y) values of the position vector. If the covariances are non-zero, the angle between the major axis of the ellipse and the x axis of the coordinate system is computed from[8]

$$\varphi = \frac{1}{2}\arctan\left(\frac{2\sigma_{xy}}{\sigma_x^2 - \sigma_y^2}\right) \tag{17}$$

and the lengths of the major (a) and minor (b) axes of the ellipse as

$$a = \frac{\left(\sigma_x^2 + \sigma_y^2\right)}{2} + \sqrt{\frac{\left(\sigma_x^2 - \sigma_y^2\right)^2}{4} + {\sigma_{xy}}^2}, \tag{18}$$

$$b = \frac{\left(\sigma_x^2 + \sigma_y^2\right)}{2} - \sqrt{\frac{\left(\sigma_x^2 - \sigma_y^2\right)^2}{4} + {\sigma_{xy}}^2}. \tag{19}$$

Note that these axes' lengths correspond to the standard error ellipse, where the least-squares estimate falls with a confidence of 39.4%. To obtain a 95% confidence region, the length of the ellipse axis is just multiplied by a factor 2.447. This multiplicative factor is determined from the chi-square distribution.

https://doi.org/10.1017/S0263574713000660 Published online by Cambridge University Press

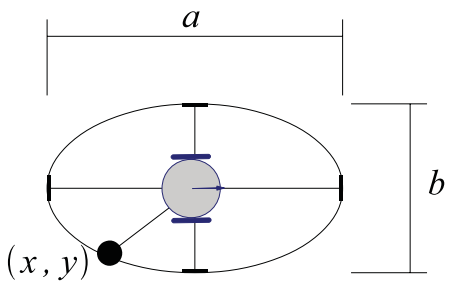


Fig. 3. (Colour online) A point $(x, y) \in$ ellipse.

5. Laser-Interferometry-Based Calibration

5.1. Systematic error calibration

The current robot configuration is estimated by continuously calculating Eq. (1) using the available measurements from the encoders. The proposed calibration methodology is aimed at minimising the reconstruction error related to the mismatching between actual and calculated paths. In other words, the object is to find the best calibration parameters that minimise the odometric error from a set of all feasible solutions. Thus, $C = [c_d \quad c_r]$ or $C = [c_l \quad c_r \quad c_W]$ are the variables to be found. This process can be formally described as

$$\min_{C \in \mathbb{R}^n} f_e(C), \tag{20}$$

where $f_e(C)$ is a nonlinear objective function from $\mathbb{R}^n$ to $\mathbb{R}$. Depending on the available external measurement system, the robot's pose can be measured during the motion or after the motion. The total error function can be mathematically expressed as the norm of the error vector $[e_X \quad e_Y \quad e_\theta]$ given by

$$f_e(C) = \sum \sqrt{e_X(C)^2 + e_Y(C)^2 + e_\theta(C)^2}. \tag{21}$$

The error function can be continuously calculated from the data set; for simplicity, only the final position of the robot was used for the function. In this study, the implementation of the error function consists of three parts:

1. The experimental data from the encoders and the real position are retrieved.
2. The final position is calculated using the current calibration parameters.
3. The error is evaluated for that particular set of data.

The optimisation algorithm used is the Nelder–Mead simplex method.[5] This is a direct search method that does not use numerical or analytic gradients. The starting calibration parameters are set as $C = [1 \quad 1]$ for the two-parameter model and $C = [1 \quad 1 \quad 1]$ for the three-parameter model. Once the best set parameters are determined from the data set, there is still likely to be a certain amount of error remaining. This remaining error after systematic calibration is the previously defined non-systematic error.

5.2. Error propagation parameters identification

A similar process can be used in order to fine-tune the error propagation functions defined in Eqs. (15) and (16). A new nonlinear objective function is defined to deal with the new requirements. Now it is important that the robot's pose remains near to the border of the error ellipse defined by Eqs. (17)–(19). Let us consider an arbitrary point $P = (x, y)$ and an ellipse centred at $(0, 0)$ with a and b as the major and minor axes, respectively. P lies on the ellipse if $\frac{x^2}{a^2/4} + \frac{y^2}{b^2/4} = 1$, as shown in Fig. 3. The error function is constructed by considering points close to the ellipse and can be expressed by

$$f_e(K) = \sum \left\| \frac{x^2}{a^2/4} + \frac{y^2}{b^2/4} - 1 \right\|. \tag{22}$$

https://doi.org/10.1017/S0263574713000660 Published online by Cambridge University Press

Table I. Speed symbols.

Symbol	Left speed (mm/s)	Right speed (mm/s)
○	34.5	34.5
×	69.0	69.0
·	34.5	69.0
+	69.0	34.5

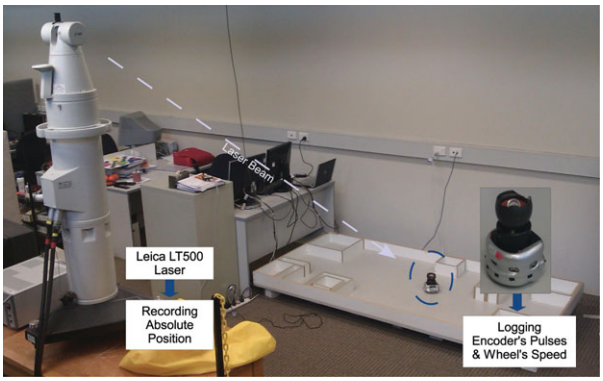


Fig. 4. (Colour online) Experimental set-up for the laser-based calibration.

Note that in most cases the error ellipse is not centred at (0, 0), then P has to be aligned with ellipse coordinates by translating and rotating the point. To find $K = [K_{rc} \quad K_{lc}]$, or $K = [K_{rl} \quad K_{ll}]$, the error function is implemented in the previously described fashion.

6. Experiment and Results

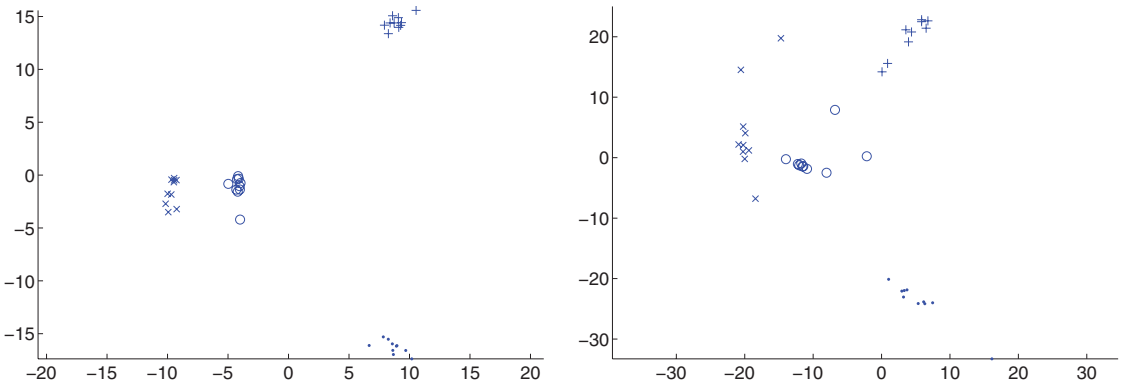
The apparatus used to measure distance is a Leica LT500 laser shown in Fig. 4. The laser can measure up to 1000 points per second with an accuracy of ± 25 μm.While the robot is able to produce encoder's pulse readings and/or current speed of each wheel at 20 Hz. It is possible to execute a set of predefined trajectories recording the internal odometry against external measurements. The orientation is taken before and after the robot's motion with a laser pointer located on top of the robot. The pointer projects the orientation of the robot onto the wall. The collected data are gathered in four groups, each group representing a combination of right and left speed. Table I shows the symbols used to represent each speed combination.

6.1. Calibration results

The uncalibrated data for pulse and speed logging are shown in Figs. 5(a) and 5(b). The total error using pulses was 518.06 while that using speed data was 800.55. After applying the optimisation method for the two-parameter model, $C = [1.0368 \quad 1.0961]$ was obtained for encoder's pulses with a total error of 164.14. $C = [1.0822 \quad 1.1129]$ was obtained for wheel speed with a total error of 250.13. The calibrated data for pulse and speed recordings using the two-parameter model are shown in Figs. 6(a) and 6(b). Note that pulses are more reliable than speed data. Figures 6(c) and 6(d) show the calibrated data for the three-parameter model. $C = [1.0378 \quad 1.0351 \quad 0.9454]$ was obtained for encoder's pulses with a total error of 159.22. $C = [1.0805 \quad 1.0832 \quad 0.9727]$ was obtained for wheel speed with a total error of 248.06. The three-parameter model presented less error than the two-parameter model.

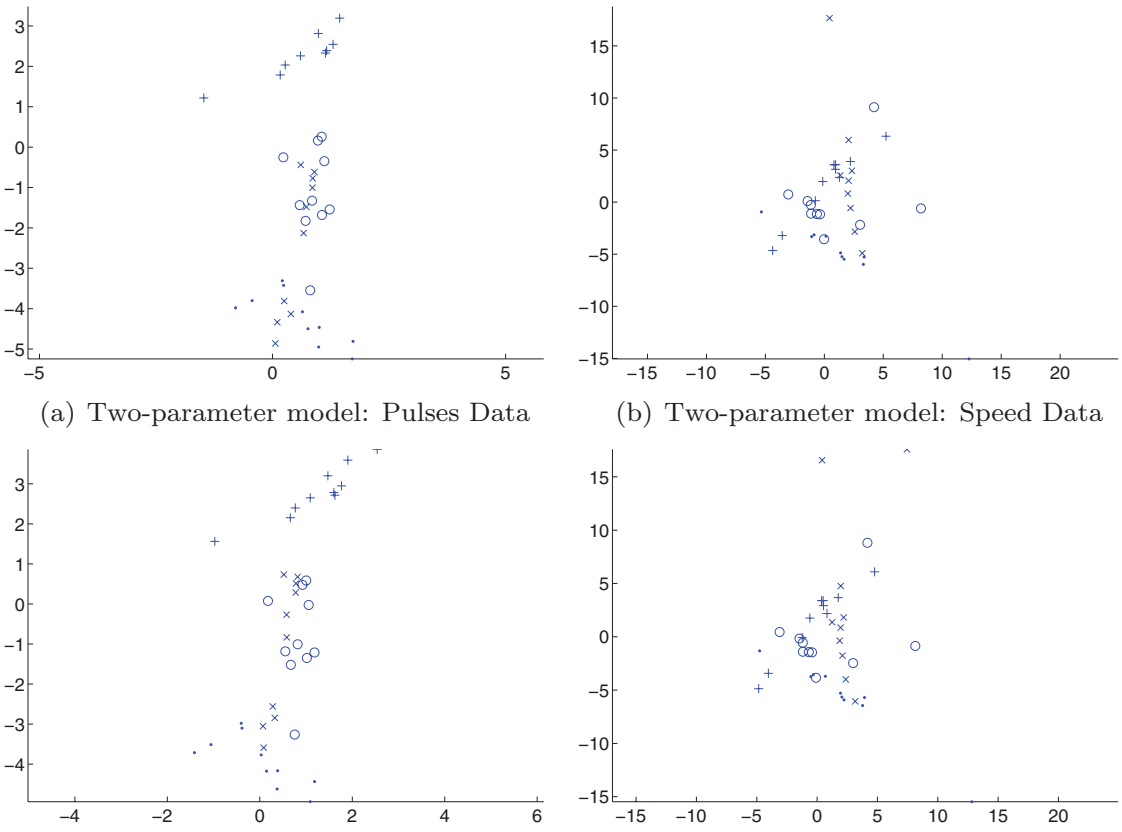
In general, the total error using pulses was lower than the total error using speed data. After applying the proposed calibration method for the two-parameter and three-parameter models, a reduction in the total error was achieved for both models. It is noticeable that the three-parameter model presented less error than the two-parameter model. The three-parameter model is more accurate because the measurement error of each wheel and the distance between themselves are described independently, while the two-parameter model describes all those errors in terms of total displacement and orientation.

https://doi.org/10.1017/S0263574713000660 Published online by Cambridge University Press



(a) Pulses Data (b) Speed Data

Fig. 5. (Colour online) Residuals (mm) before calibration.



(a) Two-parameter model: Pulses Data (b) Two-parameter model: Speed Data

(c) Three-parameter model: Pulses Data (d) Three-parameter model: Speed Data

Fig. 6. (Colour online) Residuals (mm) after calibration.

The proposed calibration is tested during a complex trajectory defined in Fig. 7. The initial error for pulse data is 34% smaller than the error for speed data. The three-parameter model reduced the errors for the entire trajectory to an error of 55.3 for pulse data and 56.6 for speed data, while the two-parameter model decreased the errors to 68.03 for pulse data and 68.24 for speed data. The method described above has a number of advantages compared with the well-known UMBmark method.[3] First, the proposed method calibrates the values of each wheel and the wheel base, whereas the UMBmark method finds only their wheel ratio, which can result in an uncertainty in the estimation of the distance travelled. Another advantage is that it does not require a particular shape of path; it can use paths with the same characteristics as the robot follows in its normal use.

https://doi.org/10.1017/S0263574713000660 Published online by Cambridge University Press

Table II. Error propagation parameters.

Data	$\mathbf{C_{u_k}}$	$f_e(K)$
Pulses	$\begin{bmatrix} 5.17 & 0 \\ 0 & 24.22 \end{bmatrix}$	22.28
	$\begin{bmatrix} 0.35N_r & 0 \\ 0 & 1.15N_l \end{bmatrix}$	24.98
Speed	$\begin{bmatrix} 27.49 & 0 \\ 0 & 117.17 \end{bmatrix}$	22.76
	$\begin{bmatrix} 1.05V_r & 0 \\ 0 & 2.48V_l \end{bmatrix}$	25.48

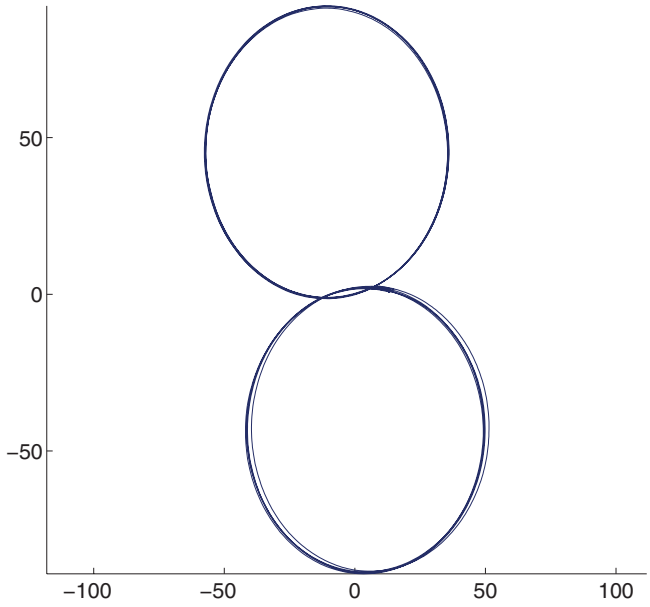


Fig. 7. (Colour online) A complex trajectory: the number eight.

6.2. Parameter estimation

Table II shows the results of the error propagation parameter estimation. The best function found was a constant set of parameters using the pulse formulation. In general, the total error using pulses was lower than that using speed data.

7. Conclusion

The position of a robot can be represented by the pose vector $[x\,y\,\theta]$. There is always an error associated with the movement of the autonomous platform. The imprecision in the position estimate is due to errors in the sensory system used to determine such estimations as well as un-modelled factors in the vehicle model. These errors are measured from data derived from experimentation and then calibrated with the proposed calibration methodology summarised as follows:

1. Setup an absolute measurement system such as the laser-based system described in this paper.
2. Generate a simple trajectory for the robot.
3. Execute the path, recording internal odometric data against the external measures.
4. Minimise the error function to get the calibration vectors.

The paper also proposed a way to obtain a closed-form expression for the position uncertainty, by means of a covariance matrix, when position estimates are being obtained using internal sensors. The proposed method is tested using a differential drive platform. We then particularise the formulation

https://doi.org/10.1017/S0263574713000660 Published online by Cambridge University Press

to obtain a close form for the covariance matrix representing the measure of position uncertainty for a given autonomous vehicle consisting of a non-holonomic architecture.

Acknowledgements
This work was supported by an Australian Research Council (ARC) Linkage grant (LP0668052). The authors thank Floorbotics International for its support.

References

1. G. Alici and B. Shirinzadeh, "A systematic technique to estimate positioning errors for robot accuracy improvement using laser interferometry based sensing," *Mech. Mach. Theory* **40**(8), 879–906 (Aug. 2005).
2. G. Antonelli, S. Chiaverini and G. Fusco, "A calibration method for odometry of mobile robots based on the least-squares technique: Theory and experimental validation," *IEEE Trans. Robot.* **21**(5), 994–1004 (Oct. 2005).
3. J. Borenstein and L. Feng, "Umbmark: A Benchmark Test for Measuring Odometry Errors in Mobile Robots," *SPIE Conference on Mobile Robots*, Philadelphia (22–26 Oct. 1995).
4. P. Goel, S. I. Roumeliotis and G. S. Sukhatme, "Robust Localization Using Relative and Absolute Position Estimates," **In**: *Proceedings of the IEEE/RSJ International Conference on Intelligent Robots and Systems*, vol. 2, Kyongju, South Korea (17–21 Oct. 1999), pp. 1134–1140.
5. J. C. Lagarias, J. A. Reeds, M. H. Wright and P. E. Wright, "Convergence properties of the Nelder–Mead simplex method in low dimensions," *SIAM J. Optim.* **9**(1), 112–147 (1998).
6. A. Martinelli and R. Siegwart, "Estimating the Odometry Error of a Mobile Robot during Navigation," *European Conference on Mobile Robots*, Warsaw, Poland (4–6 Sep. 2003).
7. N. Roy and S. Thrun, "Online Self-Calibration for Mobile Robots," **In**: *IEEE International Conference on Robotics and Automation*, vol. 3, Detroit, MI, USA (10–15 May 1999) pp. 2292–2297.
8. R. C. Smith and P. Cheeseman, "On the representation and estimation of spatial uncertainty," *Int. J. Robot. Res.* **5**(4), 56–68 (1986).
9. P. L. Teoh, B. Shirinzadeh, C. W. Foong and G. Alici, "The measurement uncertainties in the laser interferometry-based sensing and tracking technique," *Measurement* **32**(2), 135–150 (2002).

https://doi.org/10.1017/S0263574713000660 Published online by Cambridge University Press